Fibers and Polymers 2018, Vol.19, No.4, 905-913
DOI 10.1007/s12221-018-7902-z

ISSN 1229-9197 (print version)
ISSN 1875-0052 (electronic version)

Melt-spun Liquid Core Fibers: A CFD Analysis on Biphasic Flow in Coaxial Spinneret Die

Mohammadreza Naeimirad[1]* and Ali Zadhoush[2]

[1]*Department of Materials and Textile Engineering, Faculty of Engineering, Razi University, Kermanshah 67149-67346, Iran*
[2]*Department of Textile Engineering, Isfahan University of Technology, Isfahan 84156-83111, Iran*
(Received November 4, 2017; Revised February 4, 2018; Accepted February 8, 2018)

Abstract: Simulation of co-flowing behavior in a coaxial geometry (based on the designed spin pack) has been performed using properties of two immiscible liquids to represent flowing regime while passing through the spinneret for production of liquid core fiber (LCF) by one single step high-speed melt-spinning process. Computational Fluid Dynamics (CFD) simulations confirmed the continuous liquid core channel, obtained in bicomponent melt-spinning of LCF. Also different interface morphologies could be observed: from jetting to dripping and transition core-annular regime, based on the simulation parameters, affecting the driving forces. Results showed different co-flow regimes by systematic variation in non-dimensional parameters (flow rate ratio, viscosity ratio, Reynolds number, Weber number and Capillary number), individually. Also diameter of the core liquid is reduced in a logarithmic mode by increasing the outer liquid's flow rate. Flowing morphologies at different conditions were plotted in 2D state diagrams, illustrating transition from dripping to jetting regime by changing two different parameters. This CFD analysis bears potential for simple ways of controlled jet breakup in microfluidic devices, which currently primarily rely on Rayleigh-Taylor breakup. Notably this work highlights the melt-flow regime in the spinneret to realize developed fiber core structures at different conditions during bicomponent melt-spinning. Using various materials with different properties in liquid core fiber production promises many applications for this new generation fiber in very near future.

Keywords: Computational fluid dynamics, Co-flow regime, Melt-spinning, Droplet formation, Jetting

Introduction

The scientific analysis of co-flowing liquids has started from a long time ago and its understanding is still not complete due to the mathematical complexity of the underlying physical theories [1,2]. The flowing behavior of the inner liquid (disperse phase) and its transition from jetting to dripping was an interesting subject for studying [3-5] particularly in microfluidic devices where droplet formation [6,7] has become a key for many applications [8-10]. The stability of co-flow is also important in many industrial processes e.g. food and cosmetic industry [4], polymer processing [11,12] and core/sheath bicomponent fibers melt-spinning [13-15].

The co-flowing behavior of liquid jets is reviewed by Eggers *et al.* [3], emphasizing the importance of non-dimensional numbers e.g. Reynolds, Weber and Capillary number which depend on viscosity, flow rate and interfacial tension of two liquids flowing in coaxial channels with defined dimensions. The Rayleigh-Plateau instability model [1,2] describes jet breakup driven by interfacial tensions. Co-annular flowing topology is also investigated by Meister *et al.* [16,17] and other researchers [18,19]. Cramer *et al.* [4] experimentally studied the influence of different parameters (e.g. flow rate and viscosity ratio) on dripping behavior of two immiscible liquids, flowing through two coaxial channels. They investigated whether the drops peel off directly at the needle tip (dripping) or break off from liquid jets (jetting). They realized that increasing the velocity of the continuous outer phase and lowering the interfacial tension cause a decrease in the droplet size. Also all parameters enhancing the drag force of the continuous fluid and increasing the momentum of the disperse phase provoke the generation of a liquid jet. Utada *et al.* [20] investigated the dripping-to-jetting transition for a liquid passing through into another immiscible liquid. It is shown that in a co-flowing stream, the transition, in their flow device, can be characterized by a state diagram which depends on the Weber number of the inner fluid and the Capillary number of the outer fluid.

In the same line coaxial bicomponent melt-spinning is a well-established technique for production of thermoplastic fibers which two molten polymers come together within, either at the outlet of the spinneret to make core/sheath configurations [13,21-23]. Furthermore coaxial electrospinning also benefits from the same co-flow technique for production of synthetic fibers in nanoscale [24-27]. In this regard, our interest in the co-flow of two immiscible fluids is motivated by our aim, which is the processing of a molten polymer and a liquid of interest at elevated temperatures to obtain a bicomponent liquid core fiber (LCF) via high-speed melt-spinning process [28,29]. During the bicomponent fiber melt-spinning [13] the molten polymer and the core liquid are concentrically merged inside the designed spinneret (described in detail elsewhere [29,30]) using a microfluidic nozzle. Melt-spun LCFs, produced after passing several

*Corresponding author: m.naeimirad@razi.ac.ir

steps, can exhibit a range of transport or dissipation performance depending on liquid's rheological properties, which promise many applications e.g. damping [31,32], drug delivery [29, 33] etc. It is obviously impossibible to observe the buried polymer-liquid interface during real melt-spinning process. Heuberger *et al.* [5] studied the co-flow behavior of two fluids in a developed coaxial needle-tube setup by using transparent glass cylinder. They carried out this analysis in macro scale (mimmic the geometry of extrusion die). There is no observation or analysis on flowing regime during the melt-spinning trial yet. Thus we decided to realize a simulation, with the same spinning geometry (in micro scale).

CFD analysis of co-flow behavior of two immiscible liquids is a valuable tool to study the flowing regime, like droplet formation [4,34], dripping-to-jetting transition [5, 20] etc. [35]. COMSOL Multiphysics is a suitable software for tracking the interface between two immiscible fluids [36-38].

Here we present a systematic CFD analysis on co-flowing behavior of immiscible liquids in the mentioned coaxial spinneret [29] for the melt-spinning of bicomponent LCF. Experimental parameters in coaxial spinning of polymer (sheath) and liquid (core) were used as a basic data for simulation. In fact, the purpose of the present work is to give more understanding about the co-flow behavior in the micro-channel of spin-pack and highlight the effect of different parameters (e.g. viscosity ratio, flow rate ratio, Reynolds and Weber numbers etc.) on inner liquid's flowing regime. Furthermore the actual aim of this project was to produce a polymeric fiber with continuous channel filled with liquid core. Thus CFD analysis identifies the processing conditions in which desired jetting regime could be achieved.

Simulation

Theoretical Background

In a co-flow system, the core liquid can make a continuous jet (jetting) or pinch-off to the droplets (dripping), while flowing together with another immiscible liquid (sheath) as a co-flow system.

Force Balance in Co-flowing

Drop formation has three steps (filling, necking and pinching-off) which different forces affect the process. The balancing forces of a co-flow system is categorized into two groups: 1) detaching forces and 2) attaching forces [39]. As shown in Figure 1 different forces (e.g. gravity (F_G), drag (F_D), momentum (F_M), inertia (F_I), interfacial (F_Γ)) determine the flowing regimes (dripping, jetting etc.) in a co-flow system.

According to the Figure 1 F_G, F_I, F_D and F_M act as detaching forces while F_Γ is an attaching force. Balancing between aforementioned forces are presented in Equation (1).

$$F_{gravitation}+F_{inertial}+F_{drag}+F_{momentum}=F_{interfacial} \quad (1)$$

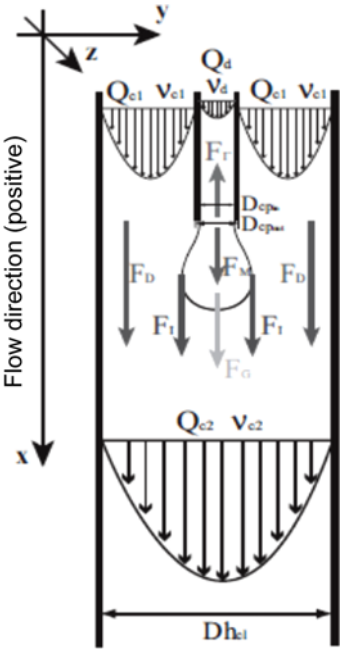

Figure 1. Force balance in a co-flow system [39].

It should be noted that interfacial tension can be determined by difference between two liquids' surface tensions (Antonov law) [40].

Non-dimensional Numbers

Based on Buckingham π theorem, different parameters can summarized in non-dimensional numbers (e.g. diameter ratio, velocity ratio (flow rate ratio), viscosity ratio, Reynolds and Weber number etc.) for a systematic study on the co-flowing behavior, which are introduced in Equations bellow, respectively:

$$Diameter\ ratio = \frac{d_o}{d_i} \quad (2)$$

$$Velocity\ ratio = \frac{v_o}{v_i} \quad (3)$$

$$Viscosity\ ratio = \frac{\mu_o}{\mu_i} \quad (4)$$

$$Re = \frac{\rho v d}{\mu} \quad (5)$$

$$We = \frac{\rho v^2 d}{\gamma} \quad (6)$$

$$Ca = \mu v/\gamma \quad (7)$$

where d is the diameter of channels, v is the velocity of fluids, μ is the viscosity, ρ is the density and γ is the interfacial surface tension between two liquids. All these

numbers are resulted from balancing between two forces, for instance Weber number is the balance between inertial and interfacial force.

In addition to the previous works on experimental study of biphasic flow [5], coaxial extrusion trial [31] and bicomponent melt-spinning process [28,29], a simulation analysis for evaluation of the co-flow behavior inside the spinneret can add more scientific value to this project.

Computational Fluid Dynamics (CFD)

A systematic CFD analysis was performed using COMSOL Multiphysics 5.2 (level set method [41]), in order to investigate the co-flowing behavior in the spin pack (with Newtonian fluid assumption, simplifying that nonlinear viscosity effects (e.g., viscoelasticity) of the sheath are not represented here). Since the experiment was performed in high temperature and high shear rate and molten polymer was placed in sheath, this simplification in CFD can predict the real co-flowing conditions [42,43]. Simulation is designed in the way to mimic the geometry of the spinneret (Figure 2) which is described in detail elsewhere [28,29] enabling the co-flow spinning of a molten polymer and a liquid. Running cases were performed by level set method, using the finest base grid and the adaptive grid option from the software menu for the computation. It took about 12 hours (average) to simulate a case using computer: Intel ® Core™ i5 - 3330 - CPU @ 3.00 GHz-3.20 GHz and RAM 4G.

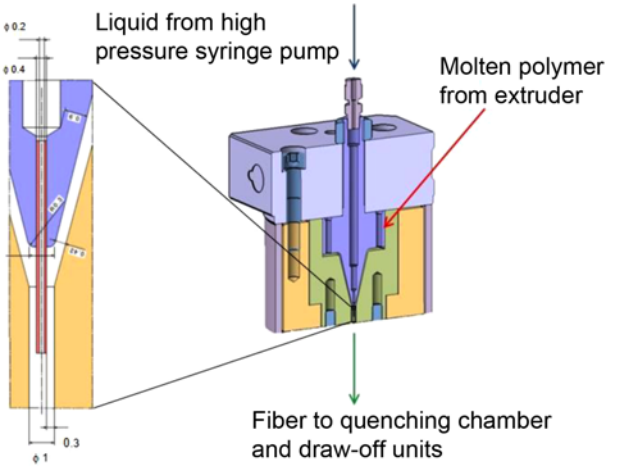

Figure 2. Sectional view of the designed spin pack with a close-up from co-flow channels of spinneret (dimensions are in mm).

It is notable that for co-flow in the mentioned spin pack, the injection ratio $\sqrt{A_i/A_o}$ in this work is about 0.2, which is larger than the ratios typically used in most previous modeling [44] and related simulation works [45,46], where the injection ratio had been between 0.002 and 0.02. Also this simulation is based on actual work, aiming to run melt-spinning trials to develop a liquid-filled core/sheath bicomponent fiber.

The spin pack geometry implies a flow column with finite size which is illustrated in Figure 3 along with the boundary conditions in 2D symmetric CFD.

According to the materials' properties (provided data sheet) and processing condition [28,29], the experimental parameters are listed in Table 1.

These parameters were used in equations (1)-(7) to calculate the non-dimensional numbers (Table 2) for simulation of the co-flow in experimental condition.

We have been able to reproduce the results for the co-flow in experimental conditions using the COMSOL Multiphysics package. Also transient morphologies were simulated, which depend strongly on the inflow boundary conditions of the two phases. In this regard all the simulation parameters (non-dimensional numbers) have been changed individually in a systematic way which is described in Table 3.

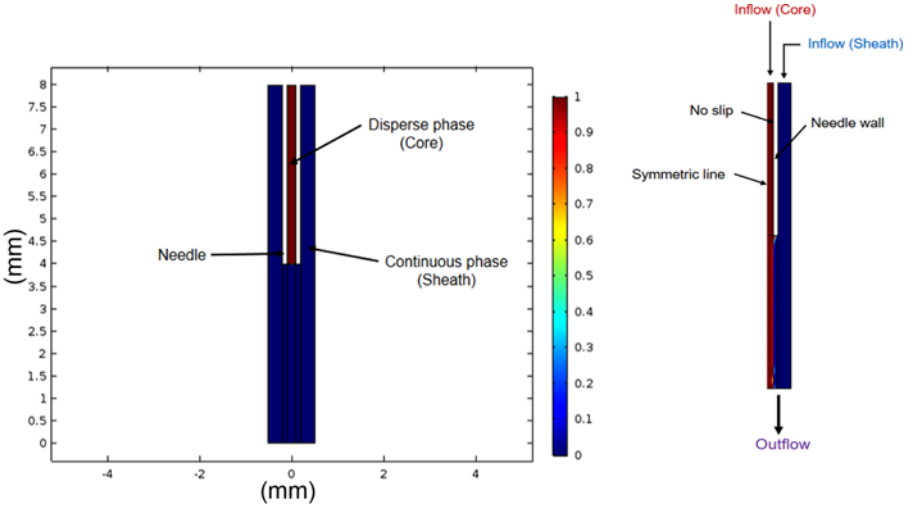

Figure 3. General geometries (left) and boundary conditions (right) in 2D symmetric simulation.

Table 1. Materials and processing parameters based on the melt-spinning experiment

Fluid/Properties	Density (g/cm^3)	Viscosity at 200 °C (Pa·s)	Flow rate (cm^3/min)	Velocity (m/S)	Interfacial tension (N/m)
Outer (Polypropylene)	0.950	150	4.5	0.113	0.014
Inner (Complex Ester)	0.910	0.003	0.66	0.355	

Table 2. Simulation parameters (non-dimensional numbers) according to the experimental trial

d_o/d_i	v_o/v_i	Q_o/Q_i	μ_o/μ_i	Re_i	We_i	Ca_o
5	0.318	6.7	50000	22.48	1.71	1210

Table 3. Range of changes for the non-dimensional parameters in simulation

Parameter	Flow rate ratio (Q_o/Q_i)	Viscosity ratio (μ_o/μ_i)	Reynolds number (Re_i)	Weber number (We_i)
Range of change	0.215-215	0.1-50000	0.02248-224.8	0.2394-23.94

Results and Discussion

For a systematic CFD analysis, the experimental data (shown in Table 1 and 2) were assumed as the standard condition and all effective parameters were changed individually, while the other parameters were constant (Table 3).

CFD Results

The CFD simulation using experimental (melt-spinning) parameters resulted in a jetting behavior through the standard co-flowing system, illustrated in Figure 4.

Figure 4 shows a jetting flow in the core channel, which the continuous liquid core, obtained in experimental process of melt-spun LCF [28,29] is a confirmation for this achievement. The higher viscosity of the outer fluid (viscosity ratio of 50000), resulting in a lower drag force, is the main reason for this jetting behavior.

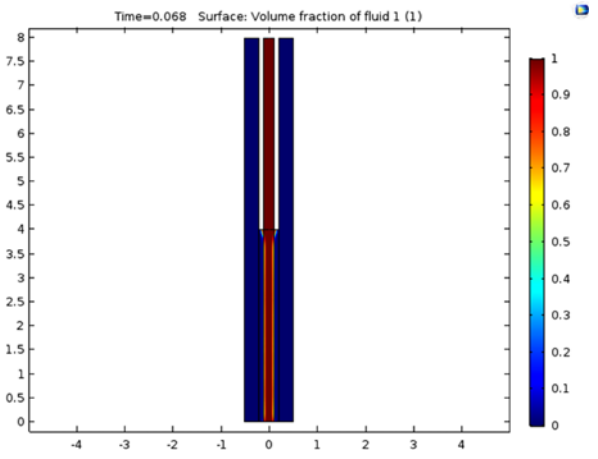

Figure 4. Co-flow behavior in standard condition (Table 2).

After analyzing the co-flow behavior in actual spinning condition, the effect of different non-dimensional parameters (e.g. flow rate and viscosity ratio, Reynolds number etc.) on flowing regimes (e.g. jetting, dripping, core-annular etc.) is discussed in next section.

Co-flow Regimes

Flow rate ratio as an important and controllable factor can affect the co-flowing behavior and diameter of the inner fluid (Figure 5).

As shown in Figure 5 increasing the flow rate ratio in actual viscosity ratio does not change the jetting behavior, while higher flow rate ratios causes lowering the inner jet diameter. This is attributed to increasing the drag force by increasing the velocity of the outer fluid (flow rate ratio) and reduction in diameter of the inner jet due to the external pressure. Variation of the inner jet at the exit point by changing the flow rate ratio is illustrated in Figure 6 which shows a logarithmic mode reduction.

As shown in Figure 7 variation of the flow rate ratio, in lower viscosity ratios, also can change the co-flow regime.

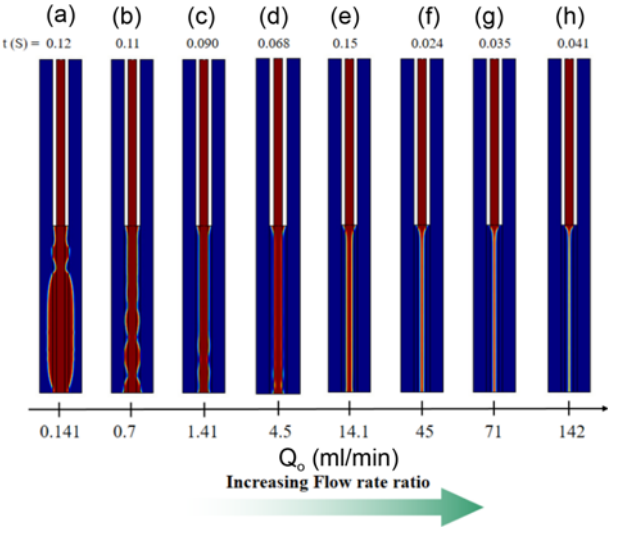

Figure 5. The effect of flow rate (velocity) ratio on co-flow behavior: μ_o=150 and μ_i=0.003 Pa.s (constant viscosity ratio of 50000), Q_i is 0.66 (ml/min) while the flow rate ratio varies (a) 0.215, (b) 1.06, (c) 2.15, (d) 6.7, (e) 21.5, (f) 67, (g) 107.5 and (h) 215.

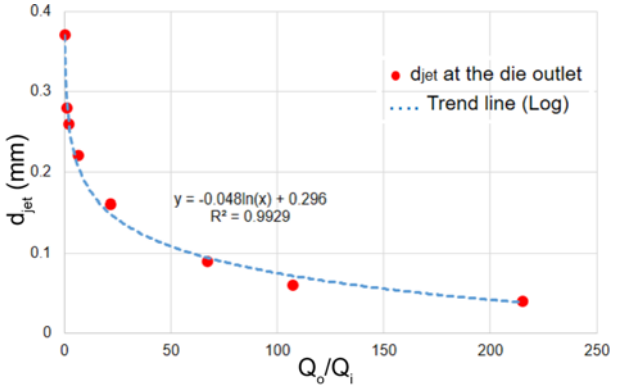

Figure 6. Diameter of the core jet at the exit point versus flow rate ratio.

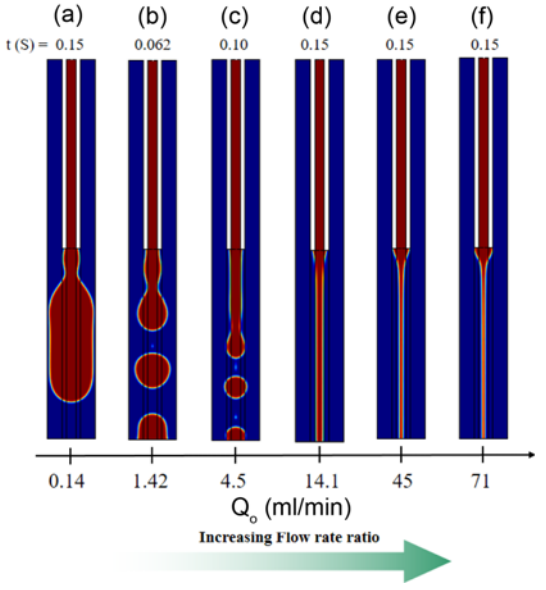

Figure 7. The effect of flow rate ratio on co-flow behavior: μ_o=0.015 and μ_i=0.003 Pa.s (constant viscosity ratio of 5), Q_i is 0.66 (ml/min) while the flow rate ratio is (a) 0.215, (b) 2.15, (c) 6.7, (d) 21.5, (e) 67 and (f) 107.5.

According to the Figure 7 droplet formation is visible at low flow rate ratios and increasing the flow rate ratio causes changing to jetting behavior in inner fluid. In other words, increasing the flow rate of continuous phase (outer fluid) creates an external force, reducing the diameter of core channel which causes small droplets to connect, leading to a jetting regime. This is in accordance with previous experimental studies [4,39,47].

Comparing Figure 5 and Figure 7 shows that variation of the flow rate ratio changes the co-flow regime in low viscosity ratios, while in high viscosity ratio (actual condition) mostly the jetting regime can be seen. Therefore the viscosity ratio is very important factor in co-flow systems.

Studying the effect of viscosity ratio was carried out by changing the shear viscosity of the outer fluid (while the inner fluid viscosity and flow rate ratio were constant) which resulted in different flowing regimes, illustrated in Figure 8.

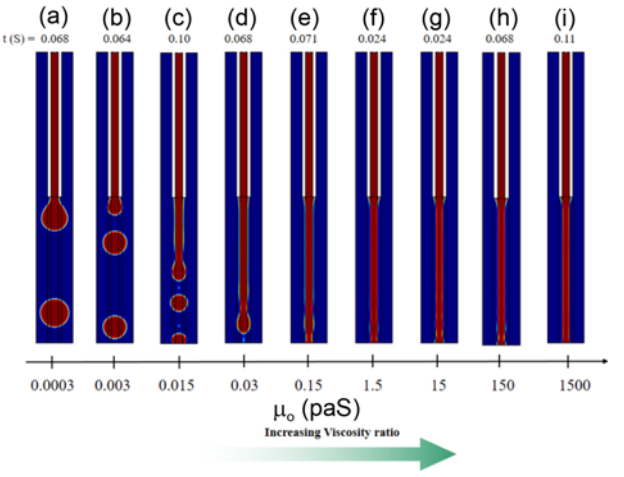

Figure 8. The effect of viscosity ratio on co-flow regime: Q_o=4.5 and Q_i=0.66 ml/min (constant flow rate ratio of 6.7), μ_i is 0.003 Pa.s and the viscosity ratio varies (a) 0.1, (b) 1, (c) 5, (d) 10, (e) 50, (f) 500, (g) 5000, (h) 50000 and (i) 500000.

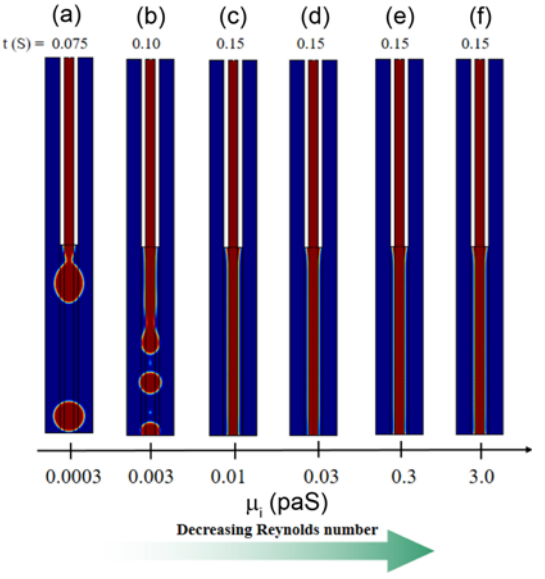

Figure 9. The effect of Reynolds number on co-flow regime by lowering it in inner fluid (Re_i) in order of (a) 224.8, (b) 22.48, (c) 6.7, (d) 2.248, (e) 0.2248 and (f) 0.02248 while the viscosity ratio is kept constant at 5, flow rate ratio is 6.7 and interfacial surface tension is 14 mN/m.

As shown in Figure 8 dripping regime is obtained in low viscosity ratios, but increasing the viscosity ratio caused in changing the flowing regime to jetting behavior. Investigating the Figure 5 and Figure 8 also indicates the importance of viscosity ratio in co-flow behavior.

The other effective non-dimensional parameter on flow behavior is the Reynolds number. The effect of Reynolds number in high viscosity ratios (more than 50) was negligible, while variation of the co-flow regime versus Reynolds number (by changing the inner fluid's viscosity) at viscosity ratio of 5 is illustrated in Figure 9.

According to the Figure 9 increasing the viscosity of the inner fluid (while the viscosity and flow rate ratios are constant) causes a laminar flow in the coaxial system. This laminar flow which is one of the characteristics in melt-spinning process changes the co-flowing behavior from dripping to the jetting regime. The reason for this variation is the increasing of detaching momentum force in higher Reynolds numbers which can conquest to attaching interfacial force in a critical point.

Weber number is the other effective non-dimensional parameter in co-flowing systems which according to the equation (12) affiliated by velocity (flow rate) and interfacial tension between two liquids (in addition to the density of liquid and channel's diameter). Figure 10 shows the flowing regimes at different Weber numbers by variation of the interfacial tension.

Lowering the attaching force (due to the increasing the interfacial tension) is the main reason for changing the co-flow regime from jetting to dripping by decreasing the Weber number (Figure 10). This phenomenon also causes bigger droplets to be formed in a lower frequency.

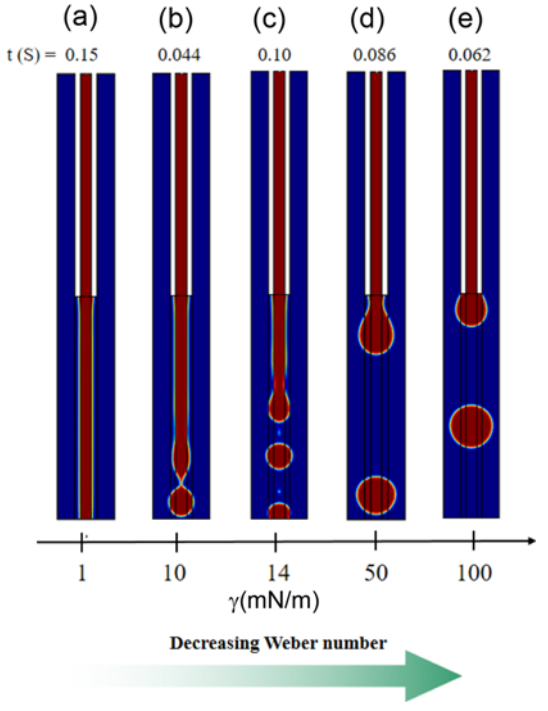

Figure 10. The impact of Weber number on inner liquid's flowing behavior: constant viscosity ratio of 5 and flow rate ratio of 6.7, while increasing the interfacial tension causes the Weber number to be changed consequently (a) 23.94, (b) 2.394, (c) 1.71, (d) 0.4788 and (e) 0.2394.

Discussion

This is resulted that all non-dimensional parameters are effective in co-flowing regime. For more investigation and better understanding on flowing behaviors at different conditions, the flowing regimes can be shown in a 2D graph by changing two different parameters.

For instance changing from dripping to a transition phase and forming a continuous jet by increasing the flow rate and viscosity ratios is illustrated in Figure 11.

According to the Figure 11(left), by increasing the viscosity ratio, dripping regime in core liquid is changed to the jetting behavior. The same behavior can be seen by increasing the flow rate ratio. As shown in transition line (core-annular regime), jetting is dominant behavior after a critical flow rate and viscosity ratio, which experimental condition will placed in this area. As shown in Figure 11 (right) increasing both the flow rates of the outer and inner fluids cause the co-flow regime to be changed from dripping to jetting. The reason for this transition is that increasing the outer fluid's flow rate increases the mass and external force around the inner fluid which causes the core channel

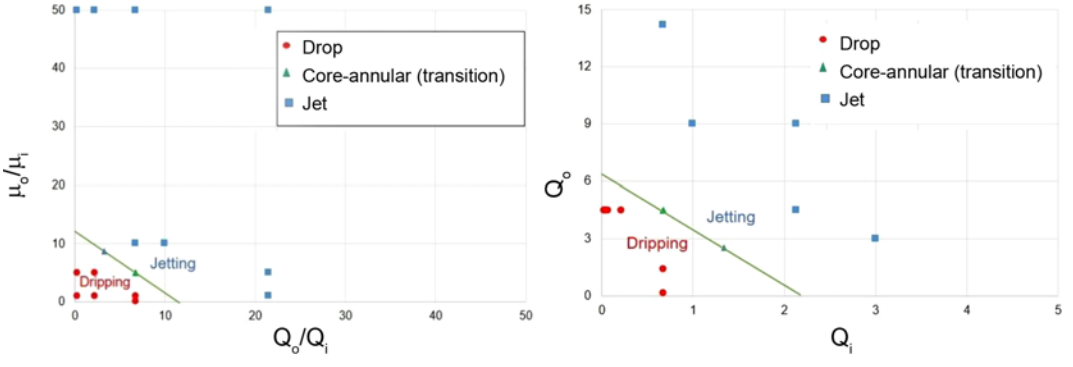

Figure 11. The variation of co-flow regimes by changing viscosity ratio versus flow rate ratio (left) and flow rate of the outer fluid versus inner fluid at constant viscosity ratio of 5 (right).

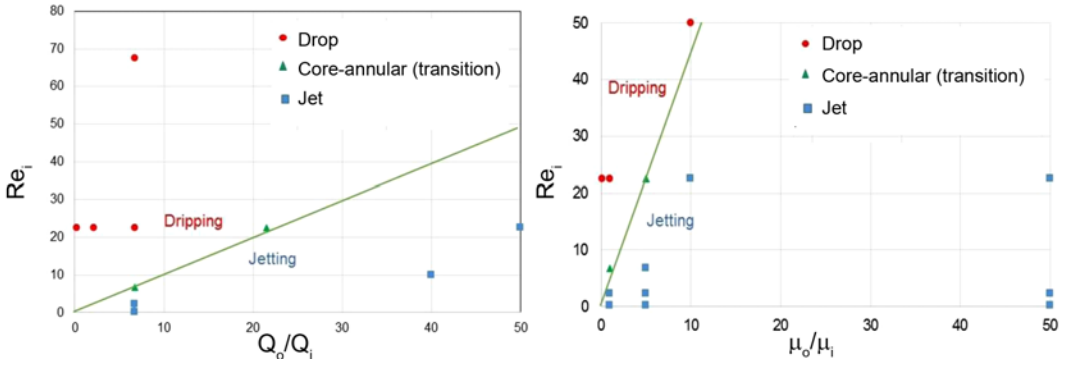

Figure 12. Variation of co-flow behaviors in biphasic flow of two immiscible liquids by changing the inner fluid's Reynolds number versus flow rate ratio, while the viscosity ratio is 5 and interfacial tension is 0.014 N/m (left) and versus viscosity ratio while the flow rate ratio is 6.7 (right).

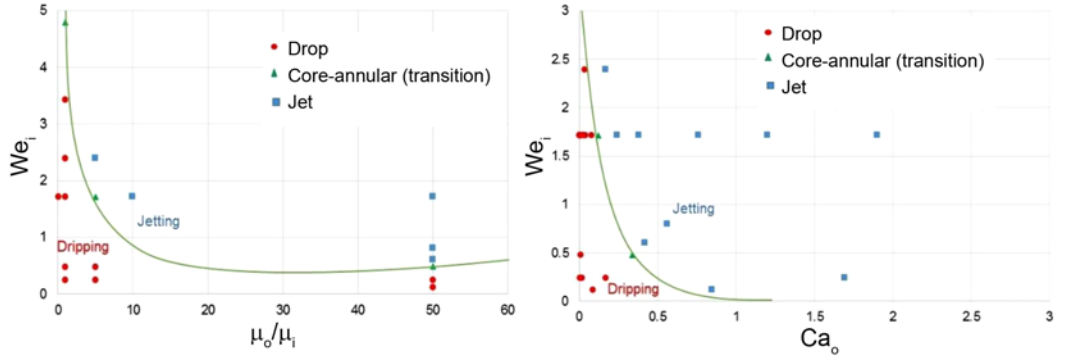

Figure 13. Variation of co-flow regimes by changing the Weber number of the inner fluid versus viscosity ratio (left) and versus capillary number of the outer fluid (right).

diameter to be decreased, leading to the jetting regime. Increasing the flow rate of the inner fluid increases its volume in the core channel and attaching forces cause a transition to jetting behavior. Reynolds number (which is the balancing between momentum and drag forces) is the other parameter with an obvious effect in low viscosity and flow rate ratios. Figure 12 shows the effect of Reynolds number along with the flow rate and viscosity ratios on co-flow regime.

According to the Figure 12(left) in addition to the flow rate ratio (mentioned before) manipulation of the Reynolds number affects the flowing behavior. Increasing the inner fluid's Reynolds number (while the flow rate and viscosity ratios are constant) causes a dripping regime due to the turbulent inner flow (more instability). In contrast, decreasing the Reynolds number (increasing the viscosity of the inner fluid) makes a laminar flow, leading to the jetting regime.

Figure 12(right) also shows a similar trend between variation of Reynolds number and viscosity ratio on co-flowing regime. Increasing the viscosity ratio and decreasing the Reynolds number resulted in a jetting regime while the inverse action causes a dripping behavior.

The other non-dimensional parameters are Weber number and Capillary number. Figure 13 shows the effect of inner fluid's Weber number versus the viscosity ratio and Capillary number of the outer fluid, separately.

According to the Figure 13(left), increasing the Weber number of the inner fluid (by lowering the interfacial tension) has the same effect as the viscosity ratio on co-flowing behavior (changing from dripping to jetting regime).

Figure 13(right) which is similar to the work by Utada *et al.* [20] indicates a similar transition (from dripping to jetting) as the inner fluid's Weber number for Capillary number of the outer fluid.

As a summary, the most important simulation result is transition from dripping to jetting regime due to the two reasons: first, increasing the attaching force and second, decreasing the detaching forces. Also the most important factor in flowing behavior is the viscosity ratio to be changed from jetting to dripping (other parameters are only effective in low viscosity ratios). Flow rate ratio, Reynolds number and interfacial tension (Weber number) are the other parameters. These results (various flowing regimes at different conditions) are in accordance with literatures [4,5, 20,39].

Conclusion

This systematic study is designed to better understand basic features of the co-flow morphology inside the bicomponent spinneret. CFD analysis showed that every individual non-dimensional parameter affects the flowing regime. It is resulted that increasing the flow rate and lowering the interfacial tension cause a decrease in the droplet size, leading to dripping-to-jetting transition. Also the inner jet shows a logarithmic reduction by increasing the flow rate ratio. Viscosity ratio is an important factor in co-flow behavior and higher viscosity of molten polymer causes a dominant rheological properties during experimental process, assuring a continuous liquid core (jetting) in melt-spun LCF which is a confirmation for previous experimental achievements. Parity parameters showed different flowing regimes in state diagrams. Increasing the inner fluid's Reynolds number caused the flowing regime to be changed from jetting to dripping behavior (in contrast with viscosity ratio) due to the increasing of detaching momentum force against the attaching interfacial force. Increasing the attaching force is the reason for changing the co-flow behavior from dripping to jetting by increasing the Weber number of the inner fluid. Increasing the Capillary number of the outer fluid has the same effect as the Weber number which are shown together in a diagram.

Acknowledgments

The authors would like to thank the Swiss Federal Laboratories for Materials Science and Technology (Empa) especially Prof. Manfred Heuberger, Dr. Rudolf Hufenus and Dr. Andres Leal for providing the liquid-filled fiber and for useful preliminary discussions. Also, they acknowledge Prof. Ahmadreza Pishevar from Department of Mechanical Engineering (IUT) for his advises in CFD analysis and Iran Ministry of Science, Research and Technology (MSRT) for the provided research scholarship (No. 331088).

References

1. J. Plateau, "Statique Expérimentale et Théorique des Liquides Soumis aux Seules Forces Moléculaires", Gauthier-Villars, Paris (France), 1873.
2. L. Rayleigh, "On the Capillary Phenomena of Jets", Proc. R. Soc. (London), 29, 71 (1879).
3. J. Eggers and E. Villermaux, *Reports on Progress in Physics*, **71**, 036601 (2008).
4. C. Cramer, P. Fischer, and E. J. Windhab, *Chem. Eng. Sci.*, **59**, 3045 (2004).
5. M. Heuberger, L. Gottardo, M. Dressler, and R. Hufenus, *Microfluidics and Nanofluidics*, 1 (2015).
6. S. Haase, *Int. J. Multiphase Flow*, **87**, 197 (2016).
7. R. M. Santos and M. Kawaji, *Int. J. Multiphase Flow*, **36**, 314 (2010).
8. G. M. Whitesides, *Nature*, **442**, 368 (2006).
9. C.-L. Lin, W.-H. Chang, C.-H. Wang, C.-H. Lee, T.-Y. Chen, F.-J. Jan, and G.-B. Lee, *Biosensors and Bioelectronics*, **63**, 572 (2015).
10. X. Li, J. Tian, and W. Shen, *ACS Appl. Mater. Interfaces*, **2**, 1 (2010).
11. M. W. Lee, S. S. Yoon, and A. L. Yarin, *ACS Appl. Mater. Interfaces*, **8**, 4955 (2016).
12. I. G. Loscertales, A. Barrero, I. Guerrero, R. Cortijo, M. Marquez, and A. Ganan-Calvo, *Science*, **295**, 1695 (2002).
13. R. Hufenus, C. Affolter, M. Camenzind, and F. A. Reifler, *Macromol. Mater. Eng.*, **298**, 653 (2013).
14. R. Hufenus, F. A. Reifler, K. Maniura-Weber, A. Spierings, and M. Zinn, *Macromol. Mater. Eng.*, **297**, 75 (2012).
15. J. Y. Lee, S. J. Oh, M. S. Lee, J. Y. Park, J. J. Ryu, and K. H. Lee, *Fiber. Polym.*, **13**, 1209 (2012).
16. B. J. Meister and G. F. Scheele, *AIChE J.*, **13**, 682 (1967).
17. B. J. Meister and G. F. Scheele, *AIChE J.*, **15**, 700 (1969).
18. M. Chinaud, K. H. Park, and P. Angeli, *Int. J. Multiphase Flow*, **90**, 1 (2017).
19. D. Albagli and Y. Levy, *Int. J. Multiphase Flow*, **16**, 929 (1990).
20. A. S. Utada, A. Fernandez-Nieves, H. A. Stone, and D. A. Weitz, *Phys. Rev. Lett.*, **99**, 094502 (2007).
21. R. Hufenus, M. Naeimirad, and A. Leal, "Melt-spun Liquid-filled Polymeric Fibers", Graz (Austria), 2015.
22. J. Francisco, B. Rodríguez, and J. Ramos, *Polymer*, **52**, 5573 (2011).
23. S. Jin, Z. Chen, B. Xin, T. Xi, and N. Meng, *Fiber. Polym.*, **18**, 1160 (2017).
24. R. E. Neisiany, J. K. Y. Lee, S. N. Khorasani, and S. Ramakrishna, *J. Appl. Polym. Sci.*, **134**, 44956 (2017).
25. M. Naeimirad, A. Zadhoush, R. Kotek, R. Esmaeely Neisiany, S. Nouri Khorasani, and S. Ramakrishna, *J. Appl. Polym. Sci.*, **135**, 46265 (2018).
26. R. E. Neisiany, J. K. Y. Lee, S. N. Khorasani, and S. Ramakrishna, *Polymer Testing*, **62**, 79 (2017).
27. S. Salimian, A. Zadhoush, M. Naeimirad, R. Kotek, and S. Ramakrishna, *Polym. Compos.*, http://www.10.1002/pc.24412 (2017).
28. M. Naeimirad, A. Zadhoush, A. Abrishamkar, A. Pishevar, and A. Leal, *Iranian Polym. J.*, **25**, 397 (2016).
29. A. A. Leal, M. Naeimirad, L. Gottardo, P. Schuetz, A. Zadhoush, and R. Hufenus, *Int. J. Polym. Mater. Polym. Biomater.*, **65**, 451 (2016).
30. L. Gottardo, R. Hufenus, M. Dressler, and M. Heuberger, "Design and Development of Liquid Filled Polymeric Fibers with Flexure Rate Viscoelastic Properties", Nuremberg (Germany), 2013.
31. R. Hufenus, L. Gottardo, A. A. Leal, A. Zemp, K. Heutschi, P. Schuetz, V. R. Meyer, and M. Heuberger, *Mater. Des.*, **110**, 685 (2016).
32. R. Esmaeely Neisiany, J. K. Y. Lee, S. Nouri Khorasani, R.

Bagheri, and S. Ramakrishna, *J. Ind. Eng. Chem*., **59**, 456 (2018).
33. R. Hufenus, A. Leal, M. Naeimirad, L. Gottardo, and M. Heuberger, "Liquid Core Melt-spun Fibers", Raleigh, NC (USA), 2015.
34. J. R. Richards, A. M. Lenhoff, and A. N. Beris, *Physics of Fluids (1994-present)*, **6**, 2640 (1994).
35. L. Arsenjuk, F. Kaske, J. Franzke, and D. W. Agar, *Inte. J. Multiphase Flow*, **85**, 177 (2016).
36. W. B. Zimmerman, "Multiphysics Modeling with Finite Element Methods", World Scientific Publishing Co. Inc., 2006.
37. Y. Li, M. Jain, and K. Nandakumar, "Numerical Study of Droplet Formation Inside a Microfluidic Flow-focusing Device", COMSOL Conference Proceeding, Boston (USA), 2012.
38. N. P. van Dijk, K. Maute, M. Langelaar, and F. Van Keulen, *Structural and Multidisciplinary Optimization*, **48**, 437 (2013).
39. M. R. Duxenneuner, "Visualization, Design, and Scaling of Drop Generation in Coflow Processes", Diss., Eidgenössische Technische Hochschule ETH Zürich, Nr. 18277, 2009, 2009.
40. G. Antonoff, *J. Phys. Chem.*, **46**, 497 (1942).
41. S. Bashir, J. M. Rees, and W. B. Zimmerman, *Chem. Eng. Sci.*, **66**, 4733 (2011).
42. C. D. Han, *J. Appl. Polym. Sci.*, **17**, 1289 (1973).
43. W. S. Lee and C. W. Park, *ASME J. Appl. Mech.*, **62**, 511 (1995).
44. B. Vempati, M. V. Panchagnula, A. Öztekin, and S. Neti, *Acta Mechanica*, **210**, 1 (2010).
45. C. Kouris and J. Tsamopoulos, *Physics of Fluids (1994-present)*, **13**, 841 (2001).
46. C. Kouris and J. Tsamopoulos, *J. Fluid Mech.*, **470**, 181 (2002).
47. J. Nunes, S. Tsai, J. Wan, and H. Stone, *J. Phys. D: Appl. Phys.*, **46**, 114002 (2013).